ASME Journal of Computational and Nonlinear Dynamics
Online journal at:
https://asmedigitalcollection.asme.org/computationalnonlinear

Nonlinear Dynamics of a Magnetic Shape Memory Alloy Oscillator

Jean M. Souza
Department of Mechanical Engineering, Federal Center for Technological Education Celso Suckow da Fonseca, CEFET/RJ, Rio de Janeiro 20.271.110, Brazil

Luciana Loureiro S. Monteiro
Department of Mechanical Engineering, Federal Center for Technological Education Celso Suckow da Fonseca, CEFET/RJ, Rio de Janeiro 20.271.110, Brazil

Marcelo A. Savi
Center for Nonlinear Mechanics, COPPE - Mechanical Engineering, Universidade Federal do Rio de Janeiro, P.O. Box 68.503, Rio de Janeiro 21.941.972, Brazil

Magnetic shape memory alloys (MSMAs) constitute a class of smart materials capable of exhibiting large magnetic field induced strain (MFIS) when subjected to magneto-mechanical loadings. Two distinct mechanisms are responsible for the induced strain: martensitic variant reorientation and phase transformation. The martensitic reorientation is the most explored mechanism presenting the advantage to potential provide high-frequency actuation since it does not rely on phase transformation cycles. Despite its capabilities and potential dynamical applications, the dynamical behavior of MSMAs is not extensively explored in the literature that is usually focused on quasi-static behavior. Thereby, the objective of this work is to analyze the nonlinear dynamics of MSMAs. In this regard, an MSMA nonlinear oscillator is investigated, exploiting the system response under different bias magnetic field levels and actuation frequencies. A phenomenological model is employed to describe the MSMA magnetomechanical behavior. Numerical simulations are carried out using the operator split technique together with an iterative process and the fourth-order Runge–Kutta method. Results show that the application of a bias magnetic field can reduce the mean displacement of the system, increasing the oscillation amplitude. Furthermore, the period of oscillation can be modified, even achieving complex behaviors, including chaos. The potential use of MSMAs to dynamical systems is explored showing the possibility to provide adaptive behaviors. [DOI: 10.1115/1.4066469]

Keywords: magnetic shape memory alloy, martensitic reorientation, nonlinear dynamics, chaos

1 Introduction

Smart materials represent a special class of materials with multiphysics coupling which means that their properties can be modified by external stimuli, such as mechanical stress, heat, magnetic, or electric fields. This remarkable characteristic enables them to be widely explored in industrial devices, as actuators, sensors, and energy harvesters. Among the most explored smart materials, piezoelectric crystals and magnetostrictive alloys possess a high bandwidth, despite a short actuation strain. On the other hand, shape memory alloys (SMAs) provide a large strain and work output, but a limited bandwidth [1,2]. Magnetic shape memory alloys (MSMAs) are a special kind of SMA that exhibit a thermomagnetomechanical coupling, being able to provide strains similar to those obtained by traditional SMAs, such as NiTi, associated with a high bandwidth. This kind of material can undergo a magnetic field induced strain (MFIS) up to 10% when subjected to magnetomechanical loadings [3]. MFIS can be generated by two different mechanisms: magnetic field induced phase transformation and martensitic variant reorientation.

The phase transformation driven by a magnetic field relies on the magnetization difference between the martensitic and austenitic phases. In the presence of a high enough magnetic field, one phase can become energetically favorable, inducing a phase transformation [1]. This phenomenon is witnessed in material systems like NiMnCoIn [4], NiMnIn, NiMnSb, and NiMnSn [5], in which the austenitic phase is ferromagnetic, presenting a higher magnetization in comparison to the martensitic phase, either paramagnetic or antiferromagnetic.

The martensitic variant reorientation mechanism is based on the nucleation and growth of specific martensitic variants favorably oriented by the magnetic field at the expense of others. Due to differences in their crystallographic structures, a macroscopic strain is observed. This phenomenon is possible in materials that possess a magnetocrystalline anisotropic energy higher than the energy required to trigger the twin boundary movement [4]. Among MSMAs, the most widely explored using the reorientation phenomenon is the Ni–Mn–Ga alloy, due to its high magneto-crystalline anisotropic energy and low twinning stress. Nevertheless, several materials have already been studied, such as FePd [6], NiCoAl [7], and NiGaFe [8]. The motion of twin boundaries, and hence the variant reorientation, is hindered by grain boundaries. Due to that, it is usually required a single crystalline material in order to induce considerable strains [1]. Thereby, the application of MSMA is limited by the cost to acquire single crystalline specimen and by the low work output density [4], compared to those of piezoelectric materials [1]. Nevertheless, it is possible to increase the MFIS in polycrystalline alloys at least up to 1% through the use of a strong texture in the sample [9].

By comparing both mechanisms, the magnetic field induced phase transformation requires a stronger magnetic field to be triggered, in the order of several Tesla [4], while the variant reorientation mechanism can be enough to be less than 1 T [10]. In

Manuscript received October 11, 2023; final manuscript received September 4, 2024; published online October 3, 2024. Assoc. Editor: Dumitru I. Caruntu.

addition, magnetic field induced phase transformation presents higher stress output [11] and a larger blocking stress when compared to the martensitic variant reorientation mechanism [12].

Another characteristic that limits the MSMA applications refers to their fatigue life. As the twin boundary advances in the reorientation process, it interacts with discontinuities and defects inside the material. This creates a pile up of dislocations and consequently stress concentration on these points, hindering further twin boundary movement and reducing their fatigue life [13]. This phenomenon occurs during actuation cycles, being more severe in single crystals where the twin boundary is more likely to travel a longer distance inside the material. Thereby, materials with a thin twin structure tend to have a longer fatigue life. The micropeening treatment has shown to be an alternative to enhance the fatigue life and yet achieve a considerable MFIS [14]. Besides, a high surface roughness is related to a short fatigue life [13]. Constraints, like sample holders, can yield opposite effects on MSMA samples. While it shortens the fatigue life for single domain crystals, it can present the opposite effect on a dense twin structure, increasing the fatigue life [14].

The magnetic field induced strain on MSMAs was first reported in 1996 [15], and since then many phenomenological models have been developed in order to describe this behavior. Among several approaches, it should be highlighted: micromagnetic models [16,17], focused on the deformation mechanism in a microscopic scale; energy models [18,19], relying on the minimization of the system's energy; phase-field models [20–22], which are able to simulate the evolution of martensitic twins and magnetic domains; and based on irreversible thermodynamics [23–25], accounting for dissipative processes through the implementation of internal state variables. Kiefer and Lagoudas [26] and Kiefer [27] developed a model based on thermodynamical principles to describe the variant reorientation phenomenon. Shirani and Kadkhodaei [28,29] proposed improvements on this model allowing the phenomenon description for all stress levels with a single set of parameters, and using a single phase diagram, regardless the magnetomechanical loading. de Souza et al. [30] developed a model for MSMAs based on the generalized standard material approach.

Since magnetic behavior allows high-frequency responses, being associated with noncontact actuation, there are several potential applications related to MSMA dynamical devices. Barker et al. [31] developed a micropump for intracranial medicine administration based on the cyclic deformation of an MSMA sample subjected to a rotating magnetic field. Saren et al. [32] tested a similar device to pump liquid and gas, working analogously to a peristaltic pump. Shi et al. [33] designed a compact actuator with a string for strain recovery and a screw for prestress. Using a similar structure, a hydraulic switching valve was studied for oil flow [34]. In addition, there have been many studies focusing on MSMA-based energy harvesting systems, of special interest for microdevices [35–38]. Vibration control is another promising application for MSMAs, since it can influence the system dissipation and natural frequency [39], providing dynamical adaptive behavior. Magnetorheological elastomer has been tested in combination with a shape memory alloy wire, to form a composite material able to reduce the limitations of SMA in stiffness tuning. This showed to be interesting for adaptive vibration absorbers [40].

Henry [41] discussed that MFIS is reduced for higher actuation frequencies, showing the importance of the dynamical analysis. Throughout reorientation cycles, eddy current as a consequence of the magnetic field, and friction due to the twin boundary motion, promote a temperature rise in the material [42]. The MFIS drop when dynamically actuated can be explained by certain MSMA phase transformation as a result of the temperature rise [14]. The MFIS tends to stabilize at lower values, since the decrease in the martensitic volume fraction weakens the heat accumulation due to twin boundary friction [43].

Despite all these potential applications, the dynamical behavior of MSMA systems is not explored in the literature that mainly treats the quasi-static loading of MSMAs. In this regard, there is a lack of works regarding the dynamical actuation of MSMAs, especially in mechanical systems. The implementation of mechanical oscillators including MSMAs elements constitute an important field of potential application in order to explore adaptive dissipation associated with hysteresis phenomena of the martensitic reorientation as well as the classical SMAs have been used in dynamical systems exploiting changes in their mechanical properties and dissipation of energy due to phase transformation [44]. In this regard, the application of the magnetic field can change the amplitude of an oscillating system, the movement pattern as period of oscillation, and even achieve chaotic-like responses. The knowledge on this field can help the development of accurate vibration control devices, actuated by magnetic field, either reducing the amplitude of an oscillating system or even its speed.

In this regard, this work deals with a dynamical investigation of MSMA systems. The phenomenological model proposed by Kiefer [27] is employed to describe the material behavior, considering the improvements proposed by Shirani and Kadkhodaei [28,29]. A single degree-of-freedom nonlinear oscillator is employed to represent the MSMA dynamical system. Numerical simulations are carried out using the operator split technique together with an iterative process and the fourth-order Runge–Kutta. The effect of the application of a bias magnetic field is investigated, focusing on the influence in the system dynamics.

2 Mathematical Model

The phenomenological description of MSMAs considers a bidimensional magnetomechanical loading composed by axial stress and transversal bias magnetic field. Irreversible thermodynamics is employed to propose a consistent model that follows the Clausius–Duhem inequality. Essentially, the total strain (ε) is composed by an elastic (ε^e) and inelastic strain (ε^r), due to the reorientation process. Therefore, the constitutive equation employs the following definition of total strain [27]:

$$\varepsilon = \varepsilon^e + \varepsilon^r \tag{1}$$

Two martensitic variants are assumed (1 is favored by the compressive stress, while 2 is favored by the transversal bias magnetic field), being represented by the volume fraction variable (ξ), which is defined based on the martensitic variant 2. The description of the inelastic strain is carried out assuming that the martensitic volume fraction is induced by a mechanical loading, and since the stress required to initiate the reorientation process is surpassed, the MSMA undergoes inelastic strain [28], according to the following equation:

$$\varepsilon^r = (1-\xi)\varepsilon^{r,\max} \tag{2}$$

where $\varepsilon^{r,\max}$ is the maximum reorientation strain that can be induced through the variant reorientation phenomenon. On this basis, the constitutive equation can be expressed by [28]

$$\varepsilon = \frac{\sigma}{E} + (1-\xi)\varepsilon^{r,\max} \tag{3}$$

where σ is the stress, E stands for the elasticity modulus of the material, and since both martensitic variants have different modulus, it is written as follows [28]:

$$E = \xi E_2 + (1-\xi)E_1 \tag{4}$$

where E_2 is the elasticity modulus of variant 2, and E_1 is the modulus for variant 1. The evolution of the martensitic volume fraction ξ is described as a function of the applied stress and magnetic field, being derived from the Gibbs free energy, depending on the reorientation direction. Therefore, a rate-independent model is proposed, which is justified by the nondiffusive characteristics of the martensitic phase transformation. The stresses required to start and to finish the

reorientation process from variant 1 to variant 2 are represented by $\sigma^{s(1,2)}$ and $\sigma^{f(1,2)}$, while the reverse transformations are represented by $\sigma^{s(2,1)}$ and $\sigma^{f(2,1)}$. It is assumed that $\mu_0 H^l$ is the limiting magnetic field below which the stresses for reverse reorientation (variant 2 to variant 1) are approximately constant, regardless the magnetic field. The terms $\sigma_0^{s(2,1)}$ and $\sigma_0^{f(2,1)}$ are, respectively, the critical stresses in which reorientation from variant 2 to variant 1 starts and finishes, in the absence of external magnetic field. On this basis, the reorientation process is described by the following equations:

- Reorientation from variant 1 to variant 2, $\dot{\xi} > 0$ [28]

$$\xi = \frac{1}{2}\cos\left\{-\frac{\pi\varepsilon^{r,\max}}{(h^s - h^f)}\left[\sigma + \frac{(h^f - h)}{\varepsilon^{r,\max}}\right]\right\} + \frac{1}{2} \tag{5}$$

$$\sigma^{s(1,2)} = \frac{(h - h^f)}{\varepsilon^{r,\max}} - \frac{(h^s - h^f)\cos^{-1}(2\xi_0 - 1)}{\pi\varepsilon^{r,\max}} \tag{6}$$

$$\sigma^{f(1,2)} = \frac{(h - h^f)}{\varepsilon^{r,\max}} \tag{7}$$

- Reorientation from variant 2 to variant 1, $\dot{\xi} < 0$ [28]
- If the applied magnetic field is lower than the limiting field ($\mu_0 H^l$)

$$\xi = \frac{1}{2}\cos\left\{\frac{\pi}{\left(\sigma_0^{f(2,1)} - \sigma_0^{s(2,1)}\right)}\left[\sigma - \sigma_0^{s(2,1)}\right]\right\} + \frac{1}{2} \tag{8}$$

$$\sigma^{s(2,1)} = \sigma_0^{s(2,1)} + \frac{\left(\sigma_0^{f(2,1)} - \sigma_0^{s(2,1)}\right)\cos^{-1}(2\xi_0 - 1)}{\pi} \tag{9}$$

$$\sigma^{f(2,1)} = \sigma_0^{f(2,1)} \tag{10}$$

- If the applied field is greater than the limiting field ($\mu_0 H^l$)

$$\xi = \frac{1}{2}\cos\left\{\frac{\pi}{\left(\sigma_0^{f(2,1)} - \sigma_0^{s(2,1)}\right)}\left[\sigma - \left(\sigma_0^{s(2,1)} + \frac{(h - h^l)}{\varepsilon^{r,\max}}\right)\right]\right\} + \frac{1}{2} \tag{11}$$

$$\sigma^{s(2,1)} = \sigma_0^{s(2,1)} + \frac{(h - h^l)}{\varepsilon^{r,\max}} + \frac{\left(\sigma_0^{f(2,1)} - \sigma_0^{s(2,1)}\right)\cos^{-1}(2\xi_0 - 1)}{\pi} \tag{12}$$

$$\sigma^{f(2,1)} = \sigma_0^{f(2,1)} + \frac{(h - h^l)}{\varepsilon^{r,\max}} \tag{13}$$

where h, h^l, h^s, and h^f are used to simplify the equations related to the magnetic field, representing the following terms:

$$h = \mu_0 H M^{\text{sat}} - \frac{\left(\mu_0 H M^{\text{sat}}\right)^2}{4\rho K_1} \tag{14}$$

$$h^l = \mu_0 H^l M^{\text{sat}} - \frac{\left(\mu_0 H^l M^{\text{sat}}\right)^2}{4\rho K_1} \tag{15}$$

$$h^s = \mu_0 H_0^{s(1,2)} M^{\text{sat}} - \frac{\left(\mu_0 H_0^{s(1,2)} M^{\text{sat}}\right)^2}{4\rho K_1} \tag{16}$$

$$h^f = \mu_0 H_0^{f(1,2)} M^{\text{sat}} - \frac{\left(\mu_0 H_0^{f(1,2)} M^{\text{sat}}\right)^2}{4\rho K_1} \tag{17}$$

Besides, the term M^{sat} is the magnetic saturation, $\mu_0 H_0^{s(1,2)}$ and $\mu_0 H_0^{f(1,2)}$ are the magnetic fields in which forward reorientation starts and finishes free of stress, K_1 is a constant referring to the magnetocrystalline anisotropic energy, ρ is the specific mass, $\mu_0 H$ is the applied field, and $\mu_0 H^l$ is the limiting magnetic field. For more details regarding the phenomenological model description, see Refs. [27–29].

2.1 Magnetic Shape Memory Alloy Oscillator. Consider a dynamical system depicted in Fig. 1, composed by a mass, m, connected to an MSMA element and linear viscous damping with coefficient c that represents all dissipation processes different from MSMA hysteretic behavior. The oscillator dynamics is represented by a displacement u, being subjected to an external stimulus $F(t)$, while the MSMA element is subjected to a transverse bias magnetic field. On this basis, the equilibrium is provided by

$$F(t) - F_R - F_D = m\ddot{u} \tag{18}$$

where $\dot{(\,)}$ represents time derivative, with t being the time; the external stimulus $F(t)$ is composed by a sum of a constant steady-state force due to a preload, F_C, and a harmonic force, $F_0 \sin(\omega t)$, where F_0 is the amplitude, and ω is the frequency. The MSMA element is assumed to be a bar with length L and cross-sectional area A, providing a restitution force F_R, calculated from the constitutive model; the viscous damper provides the dissipation force F_D, with a coefficient c. Therefore, it is possible to write the following equations:

$$F_R = \sigma A \tag{19}$$

$$F(t) = F_C + F_0 \sin(\omega t) \tag{20}$$

$$F_D = c\dot{u} \tag{21}$$

The steady force represents a preload applied to ensure that the material works under compression in order to allow the reorientation process to occur. On this basis, the dimensionless equations of motion are given by

$$\begin{cases} x' = v \\ v' = \left(\dfrac{1}{mL\omega_0^2}\right)\left[F_C + F_0 \sin(\Omega\tau)\right] - \left(\dfrac{\omega_n}{\omega_0}\right)^2 (x - \varepsilon^r) - \dfrac{c}{m\omega_0} v \end{cases} \tag{22}$$

where $\varepsilon^r = [1 - \xi(\sigma, H)]\varepsilon^{r,\max}$ is the inelastic strain being calculated according to the constitutive model; $\omega_n = \sqrt{(\text{EA}/L)/m}$ is related to the system natural frequency; and $\omega_0 = \sqrt{(E_2 A/L)/m}$ is a reference frequency defined when the MSMA sample is composed by the martensitic variant 2. In addition, $\Omega = \omega/\omega_0$ is the dimensionless frequency; $\tau = \omega_0 t$ is the dimensionless time; $x = u/L$ is the dimensionless displacement; and v is the dimensionless velocity. An initial setpoint is adopted to assure that the system is working under compression.

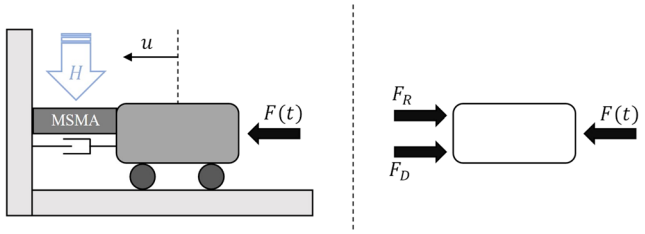

Fig. 1 Dynamical system and free body diagram identifying the forces involved

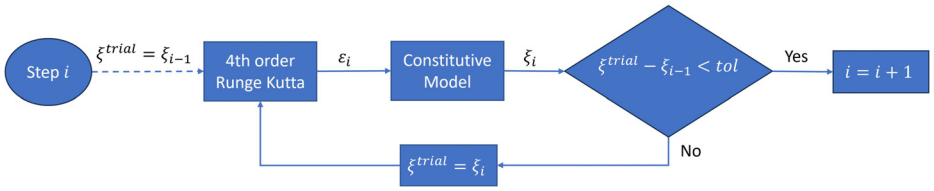

Fig. 2 Algorithm scheme based on operator split technique

Table 1 Phenomenological model and system parameters

Properties	Values	Properties	Values	Properties	Values
$\sigma_{x0}^{s(2,1)}$	0.6 MPa	$\mu_0 H_y^l$	0.055 MA/m	m	0.0225 kg
$\sigma_{x0}^{f(2,1)}$	2 MPa	M^{sat}	0.625 MA/m	L	15 mm
$\mu_0 H_{y0}^{s(1,2)}$	0.140 MA/m	E_1	2.4 GPa	A	6 mm^2
$\mu_0 H_{y0}^{f(1,2)}$	0.363 MA/m	E_2	0.4 GPa	c	10.1 N s/m
$\mu_0 H_y^{\text{cr}}$	0.6 MA/m	$\varepsilon^{r,\max}$	0.058		

3 Numerical Simulations

Numerical simulations are carried out considering an operator split approach in which dynamical problem and constitutive model are solved separately, assuming a trial state where phase transformations do not occur. The trial state establishes the predictor step where the displacement is calculated using the fourth-order Runge–Kutta method and, afterward, used as the input strain loading on the constitutive model. A corrector step is then performed, and an iterative process is adopted until variables converge through a tolerance. Figure 2 presents an algorithm scheme showing the dynamical model, represented by the fourth-order Runge–Kutta method, followed by the constitutive model and the iterative process to assure a proper convergence. Note that a trial state is assumed, using previous values. The previous step is defined by strain (ε_{i-1}) and a trial volume fraction (ξ^{trial}) that are employed to feed the Runge–Kutta method, which furnishes a displacement as output, associated with a strain (ε_i). This strain is used as input of the constitutive model, which calculates the new volume fraction (ξ_i), which is compared with the trial state. If a tolerance tol is satisfied, the time is incremented, moving to the next step. Otherwise, a new

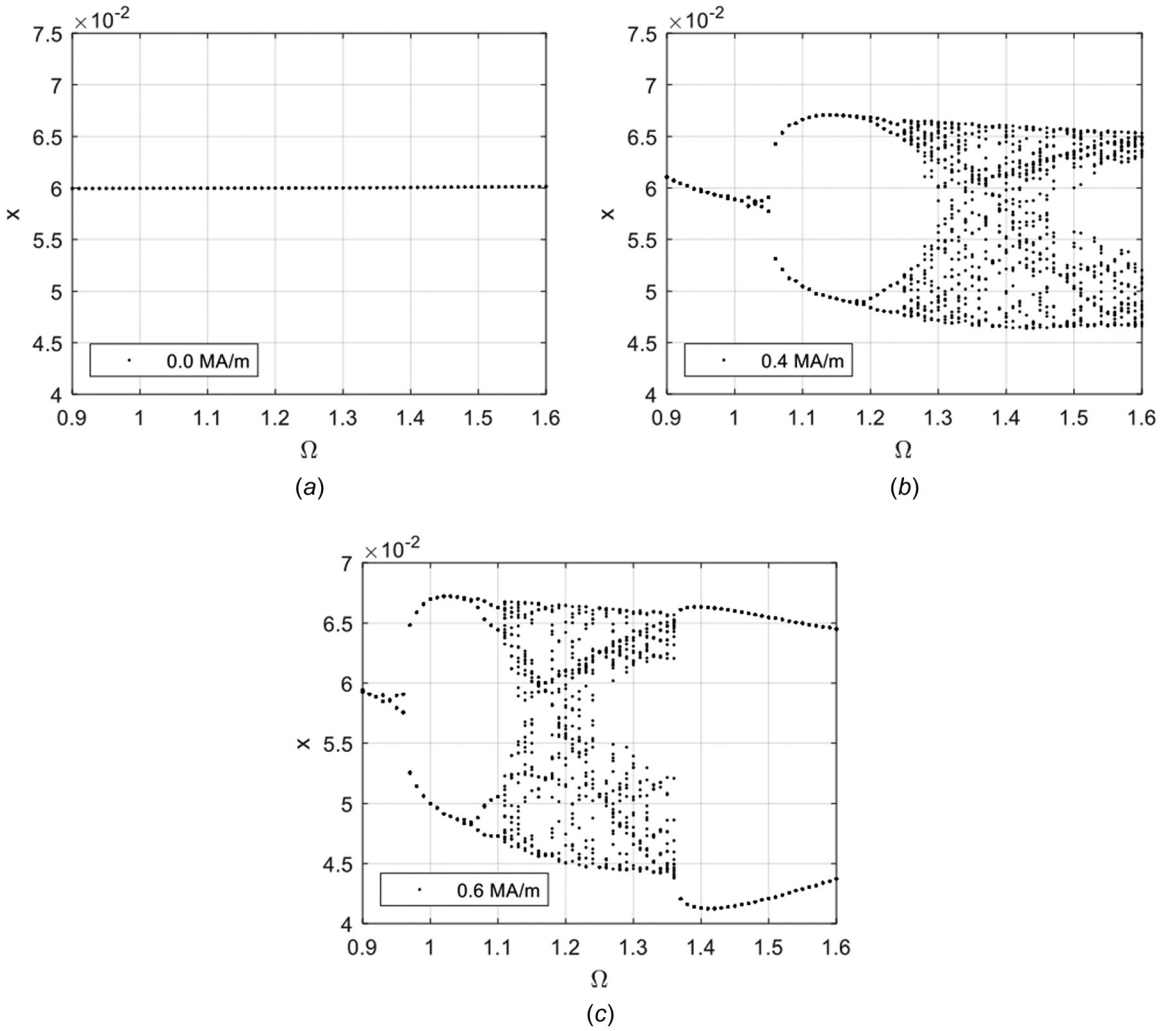

Fig. 3 Bifurcation diagrams considering the variation of the excitation frequency and different levels of the magnetic field: (*a*) 0.0 MA/m, (*b*) 0.4 MA/m, and (*c*) 0.6 MA/m

iteration is done updating the trial state and recalculating the strain and the volume fraction to repeat the process.

The system parameters for the simulations are taken from the dynamical model introduced in Ref. [45] (Table 1) together with constitutive model parameters [29]. A preload of 27 N is adopted together with a harmonic load amplitude of 30 N. Different levels of magnetic field are treated: 0, 0.4, and 0.6 MA/m. Besides, it should be noticeable that $\mu_0 H_y^{cr}$ is the critical magnetic field, above which both forward and reverse reorientation are not affected by the magnetic field.

Bifurcation diagrams provide a global view of the system dynamics. Figure 3 shows bifurcation diagrams representing the slow quasi-static variation of the forcing frequency for three levels of magnetic field. All simulations start considering MSMA subjected to a preload (27 N) resulting a volume fraction $\xi = 1$. Therefore, the initial conditions for the dynamical simulations are related to the state of the MSMA at the end of the preloading. It is noticeable that the increase of the magnetic field is related to more complex responses associated with clouds of points, Figs. 3(*b*) and 3(*c*), while a period-1 response is the typical case without magnetic field, a case without reorientation. Under the influence of the magnetic field, the system presents bifurcations from a period-1 to a period-2 response and then, to a period-4 just by increasing the excitation frequency. A chaotic-like behavior is identified in the region with a cloud of points [46].

Specific dynamical responses are now in focus considering a bias magnetic field at $\mu_0 H = 0.6$ MA/m and four different excitation frequencies. Figure 4 presents the phase-space, the time history of the volume fraction and the stress, and the stress–strain diagrams of the MSMA element. The stress–strain diagram and the volume fraction allow one to observe the martensitic reorientation processes, which are closely related to the complexity of the dynamical response. The volume fraction and stress time series are presented for a period from $\tau = 450$ to $\tau = 600$, enough to reach the steady-state behavior. Note that the system presents a period-1 response when $\Omega = 0.91$, changing to a period-2 for $\Omega = 1.0$, and period-4 when $\Omega = 1.1$. For $\Omega = 1.24$, a chaotic-like behavior is observed associated with an open curve phase-space, a Poincare map with multiple points, and irregular behavior of the volume fraction and stress time series. In addition, despite the differences in the oscillation period, the system amplitude does not vary considerably. Neither a complete reorientation back to variant 2 is

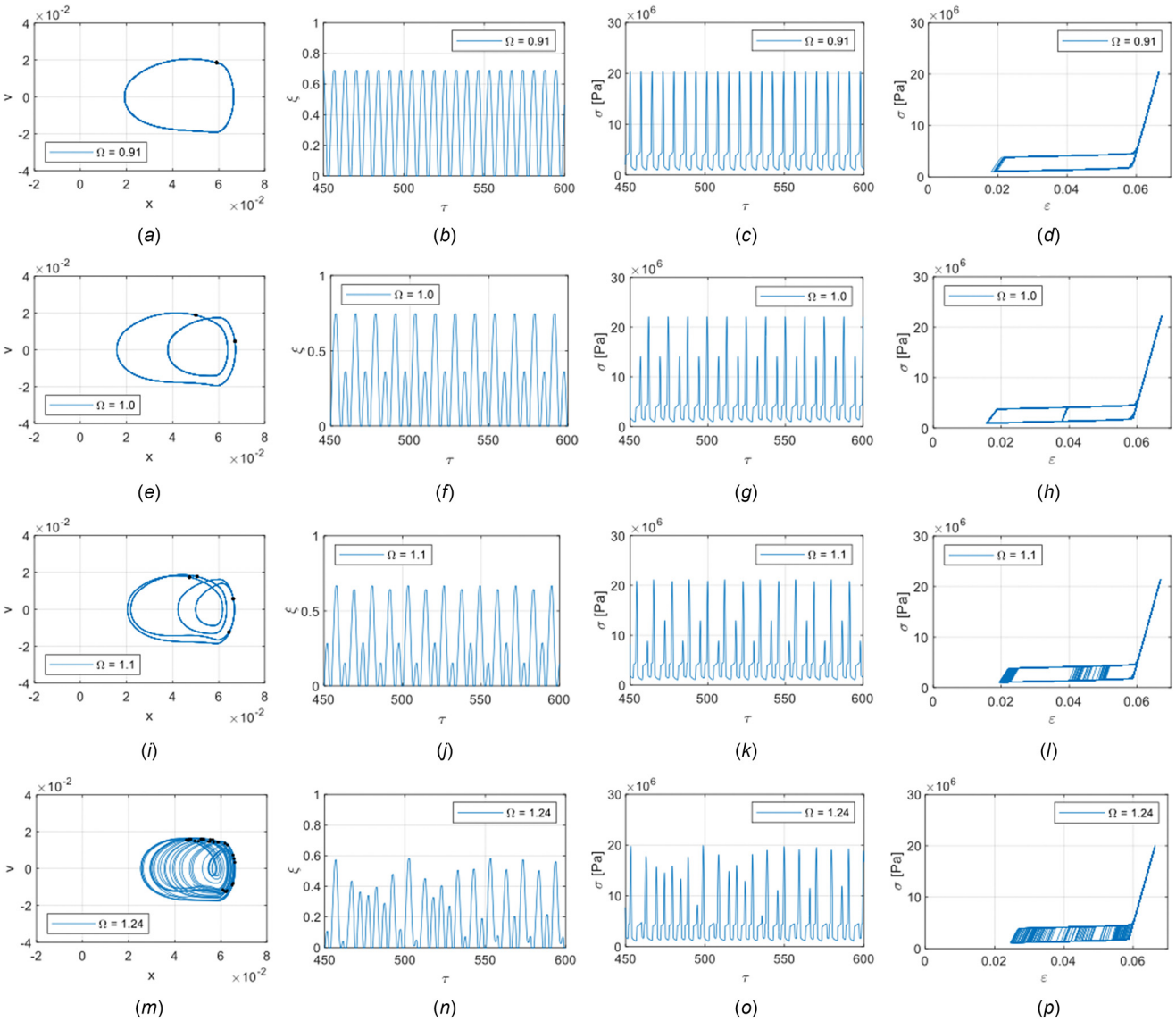

Fig. 4 Dynamical responses for $\mu_0 H = 0.6$ MA/m showing phase-space, time history of the volume fraction, time history of the stress, and stress–strain diagram: (*a*)–(*d*) Ω=0.91, (*e*)–(*h*) Ω=1.0, (*i*)–(*l*) Ω=1.1, and (*m*)–(*p*) Ω=1.24

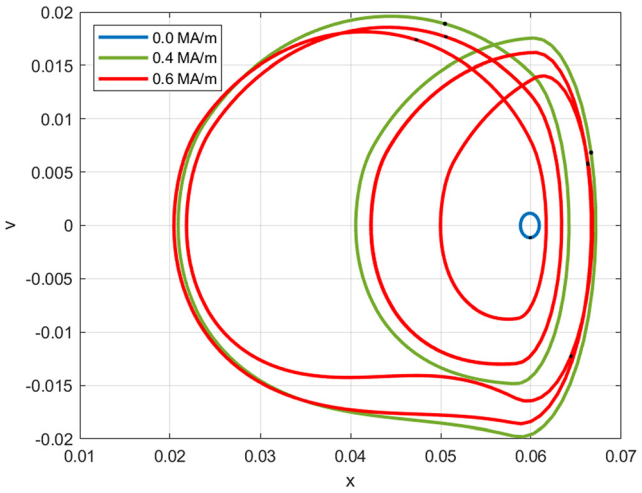

Fig. 5 Phase-space of the system response when Ω=1.1 for $\mu_0 H$=0.0 MA/m, $\mu_0 H$=0.4 MA/m, and $\mu_0 H$=0.6 MA/m

achieved. The range from $\Omega = 0.91$ to $\Omega = 1.24$ represents, in physical values, around $\omega = 2400\,\text{rad/s}$ to $\omega = 3300\,\text{rad/s}$, an interval of 900 rad/s, which is not a small variation.

It should be pointed out that deep changes can be induced in the system dynamic response just altering the bias magnetic field. Even though no considerable variation regarding the movement amplitude is observed among the four frequencies presented in Fig. 3, this behavior can be greatly modified by altering the bias magnetic field. Figure 5 shows the phase-space, when $\Omega = 1.1$ for three bias magnetic field: 0.0 MA/m, 0.4 MA/m, and 0.6 MA/m. When no magnetic field is applied, the system response presents a small amplitude when compared to the same system under 0.4 MA/m and 0.6 MA/m. On the other hand, in the presence of the two previous bias magnetic field levels, the mean displacement of the system seems to be smaller, since it reaches lower peak values of displacement periodically. Furthermore, the modulus of the peak velocities is higher when the system is subjected to 0.4 MA/m and 0.6 MA/m, comparing to the case with no magnetic field.

In order to present a deeper discussion about this kind of behavior, the mean values can be used for the analysis. In this regard, consider the mean displacement x_{mean}, which is defined as follows:

$$x_{\text{mean}} = \frac{1}{\tau}\int_{t_0}^{t_0+\tau} x\,dt \tag{23}$$

Figure 6(*a*) presents the variation of the mean displacement as a function of excitation frequency that is slowly increased, from $\Omega = 0.9$ to $\Omega = 1.6$, and assuming three bias magnetic field levels. It is noticeable that the bias magnetic field tends to induce lower mean displacements in comparison with the case without magnetic field. The case without bias magnetic field has no reorientation, leading to a constant mean displacement around $x_{\text{mean}} = 0.06$, which means that MSMA has an elastic response. For 0.4 MA/m and 0.6 MA/m, the mean displacement increases as the frequency is raised from 0.9 to 1.6, but it is still smaller than the case without magnetic field. The biggest difference of the mean displacement is observed at $\Omega = 0.9$, where for 0.0 MA/m, $x_{\text{mean}} = 0.06$ and for 0.4 MA/m, $x_{\text{rms}} = 0.038$, which is associated with a reduction of almost 37% just due to the applied bias magnetic field of 0.4 MA/m. There is a dichotomy concerning the behavior of the mean displacement and the system amplitude when the magnetic field is applied. In this regard, the amplitude around the mean displacement, mean amplitude (A_{mean}), is defined by the following equation:

$$A_{\text{mean}} = \sqrt{\frac{1}{\tau}\int_{t_0}^{t_0+\tau} (x - x_{\text{mean}})^2\,dt)} \tag{24}$$

Figure 6(*b*) shows the variation of the amplitude around the mean displacement (A_{mean}) for the same frequency sweep. While the mean position seems to be reduced with the bias magnetic field, the amplitude of the system is bigger, both in comparison with the case with 0 MA/m. The effect of the magnetic field in the amplitude for both 0.4 MA/m and 0.6 MA/m is similar, tending to decrease for higher frequencies. The enhancement of the system amplitude due to the application of the magnetic field can be explained by the inelastic strain associated with the variant reorientation process, intensified by the bias magnetic field. In the absence of a magnetic field, only elastic strain is occurring, being directly responsible for the system displacement.

On this basis, it is inferred that the increase of the bias magnetic field induces a smaller mean displacement accompanied by a larger mean amplitude. Therefore, higher magnetic field values can produce larger amplitudes in comparison with lower magnetic fields. This difference can be explained by the dissipation associated with the hysteresis loop experienced by the MSMA element. This argument can be observed in Fig. 7 that exhibits the phase-space and the stress–strain diagram for $\Omega = 1.1$, under 0.3 MA/m and 0.6 MA/m. The peak-to-peak amplitude is clearly bigger with 0.6 M/m than with 0.3 MA/m. In the scenario with 0.6 MA/m, the system undergoes a period-4 oscillation. By observing the stress–strain curves, this response is associated with different internal subloops.

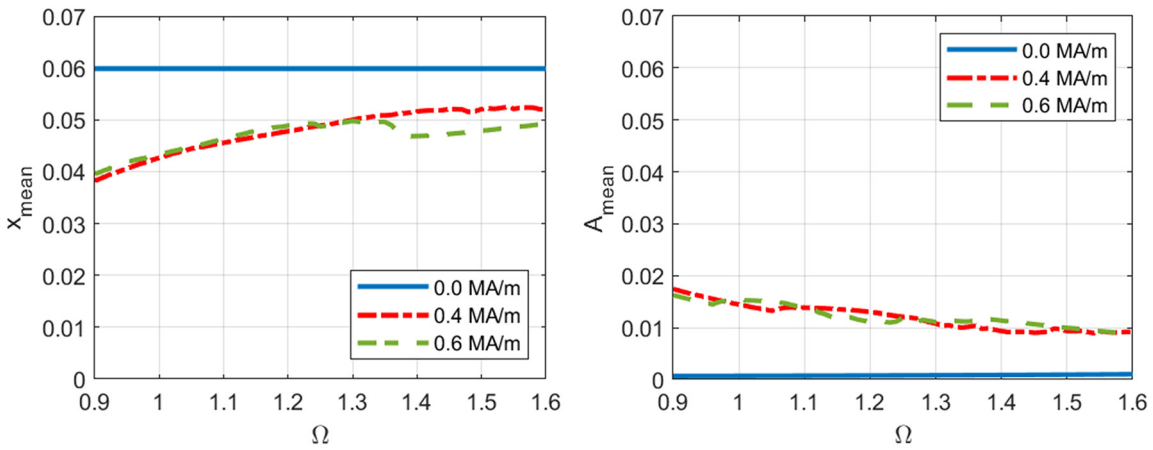

(*a*) (*b*)

Fig. 6 System response characterization by mean values with respect to frequency variations: (*a*) mean displacement and (*b*) mean amplitude

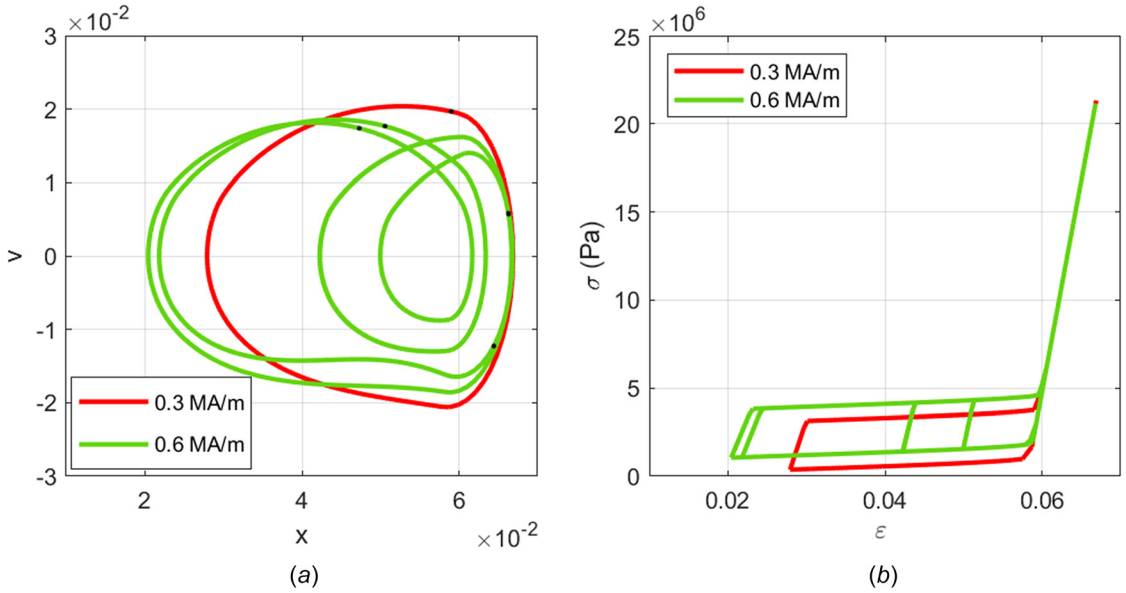

Fig. 7 System response considering Ω=1.1 and two levels of magnetic field: (*a*) phase-space and (*b*) stress–strain curve

On the other hand, the scenario with 0.3 MA/m presents a period-1 oscillation, visiting just one hysteresis loop for each period. Therefore, the dissipation with 0.3 MA/m is more intense than with 0.6 MA/m, which explains the distinct behaviors.

4 Conclusions

This work investigates the nonlinear dynamics of an MSMA system. A phenomenological model based on thermodynamic principles is adopted to describe the martensitic reorientation. The operator split technique together with an iterative process is employed for numerical simulations. The system behavior is simulated for different magnetic field levels and external stimulus characteristics. Results show that the application of the magnetic field can lead to deep dynamical behavior changes. It is possible to modify the period of oscillation and even achieve chaotic-like responses. Besides, a reduction of the system mean displacement can be achieved by increasing the excitation frequency or the magnetic field inducing a more intense variant reorientation occurring along the oscillation cycles.

Based on numerical simulations, a reduction up to 37% on the mean displacement is achieved. On the other hand, the amplitude of the displacement is greatly increased. The maximum displacement value is bigger, and the minimum displacement value is lower for the case with an applied bias magnetic field. Besides, the modulus of the peak velocities (maximum and minimum) is bigger when compared with the case without a magnetic field. These results show that the use of MSMA elements in dynamical systems confers adaptive behavior that is capable to modify their dynamical behavior through the application of a bias magnetic field.

In summary, MSMAs can promote drastic reductions of the mechanical variables, displacement and velocity, by considering the application of a bias magnetic field. On the other hand, the use of MSMA as actuator can enhance the flow rate with an increase of the magnetic field. Nevertheless, the nonlinearities involved demand a deep dynamical analysis since complex behavior can be expected, including chaos.

Acknowledgment

The authors would like to acknowledge the support of the Brazilian Research Agencies CNPq (Conselho Nacional de Desenvolvimento Científico e Tecnológico), CAPES (Coordenação de Aperfeiçoamento de Pessoal de Nível Superior), and FAPERJ (Fundação Carlos Chagas Filho de Amparo à Pesquisa do Estado do Rio de Janeiro) and through the INCT-EIE (National Institute of Science and Technology—Smart Structures in Engineering), CNPq, CAPES, and FAPEMIG (Fundação de Amparo à Pesquisa do Estado de Minas Gerais). The support of the AFOSR (Air Force Office of Scientific Research) is also acknowledged (FA9550-23-1-0527).

Funding Data

- CNPq (Conselho Nacional de Desenvolvimento Científico e Tecnológico) (Nos: 306.079/2023-2, 403.250/2023-4, and 441.460/2023-2; Funder ID: 10.13039/501100003593).
- CAPES (Coordenação de Aperfeiçoamento de Pessoal de Nível Superior) (No: 88881.974019/2024-01; Funder ID: 10.13039/501100002322).
- FAPERJ (Fundação Carlos Chagas Filho de Amparo a Pesquisa do Estado do Rio de Janeiro) (No: E-26/201.017/2022; Funder ID: 10.13039/501100004586).
- INCT-EIE (National Institute of Science and Technology—Smart Structures in Engineering) (No: 406.148/2022-8).
- AFOSR (Air Force Office of Scientific Research) (No: FA9550-23-4301-0527).

Data Availability Statement

The datasets generated and supporting the findings of this article are obtainable from the corresponding author upon reasonable request.

References

[1] Faran, E., and Shilo, D., 2016, "Ferromagnetic Shape Memory Alloys—Challenges, Applications, and Experimental Characterization," Exp. Tech., **40**, pp. 1005–1031.

[2] Savi, M. A., Paiva, A., de Araújo, C. J., and de Paula, A. S., 2016, "Shape Memory Alloys," *Dynamics of Smart Systems and Structures*, V. Lopes, Jr., V. Steffen, Jr., and M. A. Savi, eds., Springer Cham, Switzerland.

[3] Smith, A. R., Tellinen, J., and Ullakko, K., 2014, "Rapid Actuation and Response of Ni–Mn–Ga to Magnetic-Field-Induced Stress," Acta Mater., **80**, pp. 373–379.

[4] Karaca, H. E., Karaman, I., Basaran, B., Ren, Y., Chumlyakov, Y. I., and Maier, H. J., 2009, "Magnetic Field-Induced Phase Transformation in NiMnCoIn Magnetic Shape-Memory Alloys—A New Actuation Mechanism With Large Work Output," Adv. Funct. Mater., **19**(7), pp. 983–998.

[5] Sutou, Y., Imano, Y., Koeda, N., Omori, T., Kainuma, R., Ishida, K., and Oikawa, K., 2004, "Magnetic and Martensitic Transformations of NiMnX (X = In, Sn, Sb) Ferromagnetic Shape Memory Alloys," Appl. Phys. Lett., **85**(19), pp. 4358–4360.

[6] Cui, J., Shield, T. W., and James, R. D., 2004, "Phase Transformation and Magnetic Anisotropy of an Iron–Palladium Ferromagnetic Shape-Memory Alloy," Acta Mater., **52**(1), pp. 35–47.
[7] Oikawa, K., Wulff, L., Iijima, T., Gejima, F., Ohmori, T., Fujita, A., Fukamichi, K., Kainuma, R., and Ishida, K., 2001, "Promising Ferromagnetic Ni–Co–Al Shape Memory Alloy System," Appl. Phys. Lett., **79**(20), pp. 3290–3292.
[8] Oikawa, K., Ota, T., Ohmori, T., Tanaka, Y., Morito, H., Fujita, A., Kainuma, R., Fukamichi, K., and Ishida, K., 2002, "Magnetic and Martensitic Phase Transitions in Ferromagnetic Ni–Ga–Fe Shape Memory Alloys," Appl. Phys. Lett., **81**(27), pp. 5201–5203.
[9] Rogovoy, A., and Stolbova, O., 2016, "Modeling the Magnetic Field Control of Phase Transition in Ferromagnetic Shape Memory Alloys," Int. J. Plast., **85**, pp. 130–155.
[10] Zhang, S., Chen, X., Moumni, Z., and He, Y., 2018, "Thermal Effects on High-Frequency Magnetic-Field-Induced Martensite Reorientation in Ferromagnetic Shape Memory Alloys: An Experimental and Theoretical Investigation," Int. J. Plast., **108**, pp. 1–20.
[11] Yu, C., Kang, G., and Fang, D., 2018, "A Thermo-Magneto-Mechanically Coupled Constitutive Model of Magnetic Shape Memory Alloys," Acta Mech. Solida Sin., **31**(5), pp. 535–556.
[12] Haldar, K., Lagoudas, D. C., and Karaman, I., 2014, "Magnetic Field-Induced Martensitic Phase Transformation in Magnetic Shape Memory Alloys: Modeling and Experiments," J. Mech. Phys. Solids, **69**, pp. 33–66.
[13] Lawrence, T., Lindquist, P., Ullakko, K., and Müllner, P., 2016, "Fatigue Life and Fracture Mechanics of Unconstrained Ni–Mn–Ga Single Crystals in a Rotating Magnetic Field," Mater. Sci. Eng.: A, **654**, pp. 221–227.
[14] Zhang, H., Armstrong, A., and Müllner, P., 2018, "Effects of Surface Modifications on the Fatigue Life of Unconstrained Ni-Mn-Ga Single Crystals in a Rotating Magnetic Field," Acta Mater., **155**, pp. 175–186.
[15] Ullakko, K., Huang, J. K., Kantner, C., O'Handley, R. C., and Kokorin, V. V., 1996, "Large Magnetic-Field-Induced Strains in Ni_2MnGa Single Crystals," Appl. Phys. Lett., **69**(13), pp. 1966–1968.
[16] DeSimone, A., and James, R. D., 2002, "A Constrained Theory of Magnetoelasticity," J. Mech. Phys. Solids, **50**(2), pp. 283–320.
[17] James, R. D., and Wuttig, M., 1998, "Magnetostriction of Martensite," Philos. Mag. A, **77**(5), pp. 1273–1299.
[18] He, Y. J., Chen, X., and Moumni, Z., 2011, "Two-Dimensional Analysis to Improve the Output Stress in Ferromagnetic Shape Memory Alloys," J. Appl. Phys., **110**(6), p. 063905.
[19] O'Handley, R. C., 1998, "Model for Strain and Magnetization in Magnetic Shape-Memory Alloys," J. Appl. Phys., **83**(6), pp. 3263–3270.
[20] Jin, Y. M., 2009, "Domain Microstructure Evolution in Magnetic Shape Memory Alloys: Phase-Field Model and Simulation," Acta Mater., **57**(8), pp. 2488–2495.
[21] Peng, Q., He, Y. J., and Moumni, Z., 2015, "A Phase-Field Model on the Hysteretic Magneto-Mechanical Behaviors of Ferromagnetic Shape Memory Alloy," Acta Mater., **88**, pp. 13–24.
[22] Peng, Q., Huang, J., Chen, M., and Sun, Q., 2017, "Phase-Field Simulation of Magnetic Hysteresis and Mechanically Induced Remanent Magnetization Rotation in Ni-Mn-Ga Ferromagnetic Shape Memory Alloy," Scr. Mater., **127**, pp. 49–53.
[23] Chen, X., Moumni, Z., He, Y., and Zhang, W., 2014, "A Three-Dimensional Model of Magneto-Mechanical Behaviors of Martensite Reorientation in Ferromagnetic Shape Memory Alloys," J. Mech. Phys. Solids, **64**(1), pp. 249–286.
[24] Gauthier, J. Y., Lexcellent, C., Hubert, A., Abadie, J., and Chaillet, N., 2007, "Modeling Rearrangement Process of Martensite Platelets in a Magnetic Shape Memory Alloy Ni_2MnGa Single Crystal Under Magnetic Field and (or) Stress Action," J. Intell. Mater. Syst. Struct., **18**(3), pp. 289–299.
[25] Hirsinger, L., and Lexcellent, C., 2003, "Modelling Detwinning of Martensite Platelets Under Magnetic and (or) Stress Actions on Ni–Mn–Ga Alloys," J. Magn. Magn. Mater., **254–255**, pp. 275–277.
[26] Kiefer, B., and Lagoudas, D. C., 2005, "Magnetic Field-Induced Martensitic Variant Reorientation in Magnetic Shape Memory Alloys," Philos. Mag., **85**(33–35), pp. 4289–4329.
[27] Kiefer, B., 2007, "A Phenomenological Constitutive Model for Magnetic Shape Memory Alloys," Ph.D. thesis, Texas A&M University, College Station, TX.
[28] Shirani, M., and Kadkhodaei, M., 2015, "A Modified Constitutive Model With an Enhanced Phase Diagram for Ferromagnetic Shape Memory Alloys," J. Intell. Mater. Syst. Struct., **26**(1), pp. 56–68.
[29] Shirani, M., and Kadkhodaei, M., 2014, "A Geometrical Approach to Determine Reorientation Start and Continuation Conditions in Ferromagnetic Shape Memory Alloys Considering the Effects of Loading History," Smart Mater. Struct., **23**(12), p. 125008.
[30] de Souza, V. F., Savi, M. A., Monteiro, L. L. S., and Paiva, A., 2018, "Phenomenological Modeling of the Thermo-Magneto-Mechanical Behavior of Magnetic Shape Memory Alloys," J. Intell. Mater. Syst. Struct., **29**(19), pp. 3696–3709.
[31] Barker, S., Rhoads, E., Lindquist, P., Vreugdenhil, M., and Müllner, P., 2016, "Magnetic Shape Memory Micropump for Submicroliter Intracranial Drug Delivery in Rats," ASME J. Med. Devices, **10**(4), p. 041009.
[32] Saren, A., Smith, A. R., and Ullakko, K., 2018, "Integratable Magnetic Shape Memory Micropump for High-Pressure, Precision Microfluidic Applications," Microfluid. Nanofluid., **22**(4), p. 38.
[33] Shi, H., Tan, K., Xu, J., and Mei, X., 2020, "Design and Performance Analysis of Magnetic Shape Memory Alloy Actuator With a Compact Electromagnetic Coil Configuration," IEEE Trans. Magn., **56**(8), pp. 1–13.
[34] Shi, H., Liu, Z., Wang, H., and Mei, X., 2021, "Design and Performance Analysis of Hydraulic Switching Valve Driven by Magnetic Shape Memory Alloy," Adv. Mech. Eng., **13**(5), p. 168781402110169.
[35] Jing, Y., Luping, W., and Jin, X., 2020, "Design and Implementation of Vibration Energy Harvester Based on MSMA Cantilever Beam," Trans. Electr. Electron. Mater., **21**(4), pp. 399–405.
[36] Rashidi, S., Ehsani, M. H., Shakouri, M., and Karimi, N., 2021, "Potentials of Magnetic Shape Memory Alloys for Energy Harvesting," J. Magn. Magn. Mater., **537**, p. 168112.
[37] Safari, O., Zakerzadeh, M. R., and Baghani, M., 2021, "Study of a Magnetic SMA-Based Energy Harvester Using a Corrugated Structure," J. Intell. Mater. Syst. Struct., **32**(16), pp. 1855–1866.
[38] Sayyaadi, H., Mehrabi, M., and Hoviattalab, M., 2021, "Analysis and Modification of a Common Energy Harvesting System Using Magnetic Shape Memory Alloys," J. Intell. Mater. Syst. Struct., **32**(5), pp. 568–583.
[39] Mohammadsalehi, M., Zakerzadeh, M. R., and Baghani, M., 2016, "Analysis of Nonlinear Free Vibration of a Beam With Magnetic Shape Memory Alloy Elements," J. Intell. Mater. Syst. Struct., **27**(16), pp. 2216–2228.
[40] Kumbhar, S. B., Chavan, S. P., and Gawade, S. S., 2018, "Adaptive Tuned Vibration Absorber Basedon Magnetorheological Elastomer-Shape Memory Alloy Composite," Mech. Syst. Signal Process., **100**, pp. 208–223.
[41] Henry, C. P., 2002, "Dynamic Actuation Properties of Ni-Mn-Ga Ferromagnetic Shape Memory Alloys," Ph.D. thesis, Massachusetts Institute of Technology, Cambridge, MA.
[42] Pascan, O. Z., He, Y. J., Moumni, Z., and Zhang, W. H., 2015, "Temperature Rise of High-Frequency Martensite Reorientation Via Type II Twin Boundary Motion in NiMnGa Ferromagnetic Shape Memory Alloy," Scr. Mater., **104**, pp. 71–74.
[43] Pascan, O. Z., He, Y., Moumni, Z., and Zhang, W., 2016, "High-Frequency Performance of Ferromagnetic Shape Memory Alloys," Ann. Solid Struct. Mech., **8**(1–2), pp. 17–25.
[44] Enemark, S., Savi, M. A., and Santos, I. F., 2015, "Experimental Analyses of Dynamical Systems Involving Shape Memory Alloys," Smart Struct. Syst., **15**(6), pp. 1521–1542.
[45] Chen, X., and He, Y., 2020, "Thermo-Magneto-Mechanical Coupling Dynamics of Magnetic Shape Memory Alloys," Int. J. Plast., **129**, p. 102686.
[46] Savi, M. A., 2024, "Chaos Theory," *Lectures on Nonlinear Dynamics—Understanding Complex Systems*, J. R. C. Piqueira, C. E. N. Mazzilli, C. P. Pesce, and G. R. Franzini, eds., Springer, Cham, Switzerland, pp. 283–299.